

## Where to look and how to look: Combining global sensitivity analysis with fast/slow analysis to study multi-timescale oscillations



Manu Aggarwal<sup>a</sup>, Nicholas Cogan<sup>a</sup>, Richard Bertram<sup>\*,a,b</sup>

<sup>a</sup> Department of Mathematics, Florida State University, Tallahassee, FL 32306, United States

<sup>b</sup> Programs in Neuroscience and Molecular Biophysics, Florida State University, Tallahassee, FL 32306, United States

### ABSTRACT

Parameterized systems of nonlinear ordinary differential equations, the type of system that is often used in mathematical models for biological systems, can be of sufficient complexity that it can take years to appreciate the full range of behaviors that can be produced. Global sensitivity analysis is one tool that has been developed for determining which parameters have the largest impact on the behavior of the model. Thus, it provides the user with a tool to know where to look in parameter space for important changes in behavior. However, it says nothing about the underlying mechanism mediating a change in behavior. For this, other tools exist. If the system dynamics occur over multiple highly-separated time scales then one useful analysis tool is fast/slow geometric analysis, also known as geometric singular perturbation analysis. This is based on bifurcation analysis of a fast or slow subsystem, and can shed light on the influence that a parameter has on structures of either subsystem, and thus on the system dynamics. Hence, once one knows where to look in parameter space for interesting behavior, this technique describes how to look at the system to extract information about how parameter changes influence the behavior of the system. In this study, we combine the two techniques in the analysis of bursting behavior in a model of insulin-secreting pancreatic  $\beta$ -cells, with the goal of determining the key parameters setting the period of the bursting oscillations, and understanding why they are so influential. This can be viewed as a case study for combining mathematical techniques to build on the strengths of each and thereby achieve a better understanding of what most influences the range of model behaviors and how this influence is brought about.

### 1. Introduction

Global sensitivity analysis is often used to determine the impact that changes in parameters have on an output of a mathematical model. This output could be the value of an equilibrium state of the system, or a time delay before activation of some component of the model, or the amplitude or period of a limit cycle oscillation. Several global sensitivity analysis algorithms exist [16]. The advantage of these global, rather than local, sensitivity algorithms is that the effects of parameter variation are sampled over a hypercube about one or more center points in parameter space, rather than along a single dimension. While global sensitivity analysis is good at determining which parameters have the most influence on the system output, that is, at determining where to look in parameter space for changes in behavior, it is not often clear why that is, since the sampling algorithm does not reveal the mechanisms for the model dynamics. Thus, while numerical simulations can validate the results of the sensitivity analysis, the basis for the sensitivity has rarely been analyzed mathematically (but see [14]).

In this article, we apply global sensitivity analysis (Sobol' indices) to a multi-timescale model [1] for which the effects of changes in parameter values can be assessed through a geometric singular perturbation analysis. In particular, a fast/slow analysis is used in which the system is decomposed into fast and slow subsystems, based on the timescales of

the system variables [2,4,24]. We therefore combine a method for determining the importance of parameters on system output with an analysis technique that can illustrate in a geometric manner why the parameters have the impact that they do. In this model, for bursting electrical activity of insulin-secreting pancreatic  $\beta$ -cells, the output under consideration is the period of the bursting oscillation. The parameters are conductance values for ionic currents and shape parameters for activation functions. This model is chosen for the study since it is highly amenable to fast/slow geometric analysis, facilitating the analysis of parameter contributions to the system behavior. It also serves as a template for other biophysical models for bursting electrical activity (e.g., [3,7–9,12]), and therefore this study provides a road map for how global sensitivity analysis and fast/slow geometric analysis can be performed synergistically on other multi-timescale systems.

In stimulatory levels of glucose, pancreatic  $\beta$ -cells produce bursts of electrical activity (electrical impulses) that are roughly periodic with a period that can range from a few seconds to several minutes [5]. To account for this large spread of the burst period, the so-called “phantom burster” model was developed [1] that consists of two variables that vary on a fast timescale and generate the impulses, and two variables that vary on slow timescales and are responsible for packaging impulses into bursts. The first of these,  $s_1$ , has an intermediate time constant appropriate for the production of bursting with a higher frequency,

\* Corresponding author at: Department of Mathematics, Florida State University, Tallahassee, FL 32306, United States.

E-mail address: [bertram@math.fsu.edu](mailto:bertram@math.fsu.edu) (R. Bertram).

while the second,  $s_2$ , has a much larger time constant appropriate for the production of lower frequency bursting. The combination of the two slow variables with the two fast variables is sufficient to drive bursting oscillations over the full range of periods observed in  $\beta$ -cells. The fast/slow geometric analysis technique has been applied to this and a related phantom bursting model to elucidate the mechanisms for the different types of bursting: fast, medium, and slow [1,3]. However, no systematic study was performed to determine the set of parameters that have the largest impact on setting the burst period. In this report, we determine the effectiveness of global sensitivity analysis in determining these key parameters. Once the parameters have been identified, we use fast/slow geometric analysis to determine why they are so important in setting the burst period. The global sensitivity analysis thus tells us where to look, while the fast/slow analysis explains how to look for the influence of the key parameters on the model behavior.

## 2. Methods

### 2.1. The phantom bursting model

We employ a minimal model for electrical bursting in pancreatic  $\beta$ -cells [1] that has two variables, membrane potential ( $V$ ) and a fast activation variable for  $K^+$  channels ( $n$ ), for the production of electrical impulses and two variables that package the impulses into bursts. The latter two variables change on slower time scales. The first,  $s_1$ , has a time constant of 1 s, while the second,  $s_2$ , has a time constant of 2 min. Both are activation variables for slowly-activating  $K^+$  channels. The differential equations for this multi-timescale system are:

$$\frac{dV}{dt} = -(I_{Ca} + I_K + I_{s1} + I_{s2} + I_L)/C_m \tag{1}$$

$$\frac{dn}{dt} = \frac{n_\infty(V) - n}{\tau_n(V)} \tag{2}$$

$$\frac{ds_1}{dt} = \frac{s_{1\infty}(V) - s_1}{\tau_{s1}} \tag{3}$$

$$\frac{ds_2}{dt} = \frac{s_{2\infty}(V) - s_2}{\tau_{s2}} \tag{4}$$

The ionic currents are:

$$I_{Ca} = g_{Ca} m_\infty(V)(V - V_{Ca}) \tag{5}$$

$$I_K = g_K n(V - V_K) \tag{6}$$

$$I_{s1} = g_{s1} s_1(V - V_K) \tag{7}$$

$$I_{s2} = g_{s2} s_2(V - V_K) \tag{8}$$

$$I_L = g_L(V - V_L) \tag{9}$$

where the first is a  $Ca^{2+}$  current, the next three are  $K^+$  currents, and the last is a constant-conductance leakage current. The activation variables have the following equilibrium functions:

$$m_\infty(V) = \frac{1}{1 + \exp[-(22 + V)/7.5]} \tag{10}$$

$$n_\infty(V) = \frac{1}{1 + \exp[-(9 + V)/10]} \tag{11}$$

$$s_{1\infty}(V) = \frac{1}{1 + \exp[(V_{s1} - V)/\sigma_{s1}]} \tag{12}$$

$$s_{2\infty}(V) = \frac{1}{1 + \exp[(V_{s2} - V)/\sigma_{s2}]} \tag{13}$$

The time constant for  $n$  is given as the following function of  $V$ :

$$\tau_n(V) = \frac{8.3}{1 + \exp[(V + 9)/10]} \tag{14}$$

**Table 1**

Parameter values that are unchanged throughout the study.

Parameter	Value	Parameter	Value
$g_{Ca}$	280 pS	$g_K$	1300 pS
$g_L$	25 pS	$V_{Ca}$	100 mV
$V_K$	- 80 mV	$V_L$	- 40 mV
$\tau_{s1}$	1 s	$\tau_{s2}$	2 min
$C_m$	4524 fF		

**Table 2**

Parameter values for medium bursting. The interval of variation is  $\pm 5\%$  of the central values. Also shown is the total of the Sobol' indices ( $\bar{S}_i$ ) for each parameter obtained through the sensitivity analysis.

Parameter	Central Value	Interval of variation	$\bar{S}_i$
$g_{s1}$	7 pS	[6.65, 7.35]	0.019
$g_{s2}$	32 pS	[30.4, 33.6]	0.01443
$V_{s1}$	- 40 mV	[- 42, -38]	0.94976
$V_{s2}$	- 42 mV	[- 44.1, - 39.9]	0.0019
$\sigma_1$	0.5 mV	[0.475, 0.525]	0.0021
$\sigma_2$	0.4 mV	[0.38, 0.42]	0.0018

with units of ms. Parameters that are not varied throughout the study are given in Table 1.

Phase plane and fast/slow analysis are performed using the XPPAUT software package. Computer codes are available for free download from [www.math.fsu.edu/bërtram/software/islet](http://www.math.fsu.edu/bërtram/software/islet).

### 2.2. Global sensitivity analysis

For global sensitivity analysis, we estimate the Sobol' indices of the parameters with respect to the burst period, and we also analyze scatter plots of the burst period vs. the parameters. In general, given a quantity of interest (QoI) as a square-integrable function of parameters,  $y = f(p_1, \dots, p_k)$ , the total Sobol' index of a parameter  $p_i$ , denoted by  $\bar{S}_i$ , can be statistically understood as,

$$\bar{S}_i = \frac{E_{P_{-i}}(V_{P_i}(Y|P_{-i}))}{V(Y)}, \tag{15}$$

where  $P_i$  is the random variable for the parameter  $p_i$ ,  $P_{-i}$  is the vector of random variables for all parameters but  $p_i$ , and  $Y$  is the random variable for the output  $y$ . Here, it is assumed that all of the parameters are independent and uniformly distributed. The symbol  $E_{P_{-i}}(\cdot)$  is the mean over all of the parameters but  $p_i$ , and the symbol  $V_{P_i}(\cdot)$  is the variance over the parameter  $p_i$ . Eq. (15) then implies that a high  $\bar{S}_i$  indicates a high expected value of the variance in the output due to the variance in the parameter  $p_i$ , making it a *significant* parameter.

To numerically estimate the total Sobol' indices, we employ Jansen's scheme [17], which has been shown to be more efficient as compared to similar sampling-based schemes, especially when used in conjunction with quasi-random sequences [22,25]. These sequences are not actually random since they follow a specific sampling algorithm. However, they have been shown to have a low discrepancy in the context of higher uniformity in the distribution of sampling of a high-dimensional space. Using the notation from Saltelli et al. [25], we begin with generating two independent sampling matrices **A** and **B**, each of size  $N \times k$ , where  $N$  is the number of samples and  $k$  is the number of parameters. Hence, each row represents a sample and each column represents a parameter. Then, we define a matrix  $\mathbf{A}_B^{(i)}$  where all columns are from **A** except the  $i$ th column which is from **B**. Then, the total Sobol' index is estimated by,

$$\hat{\bar{S}}_i = \frac{1}{2N} \sum_{j=1}^N (f(\mathbf{A})_j - f(\mathbf{A}_B^{(i)})_j)^2, \tag{16}$$

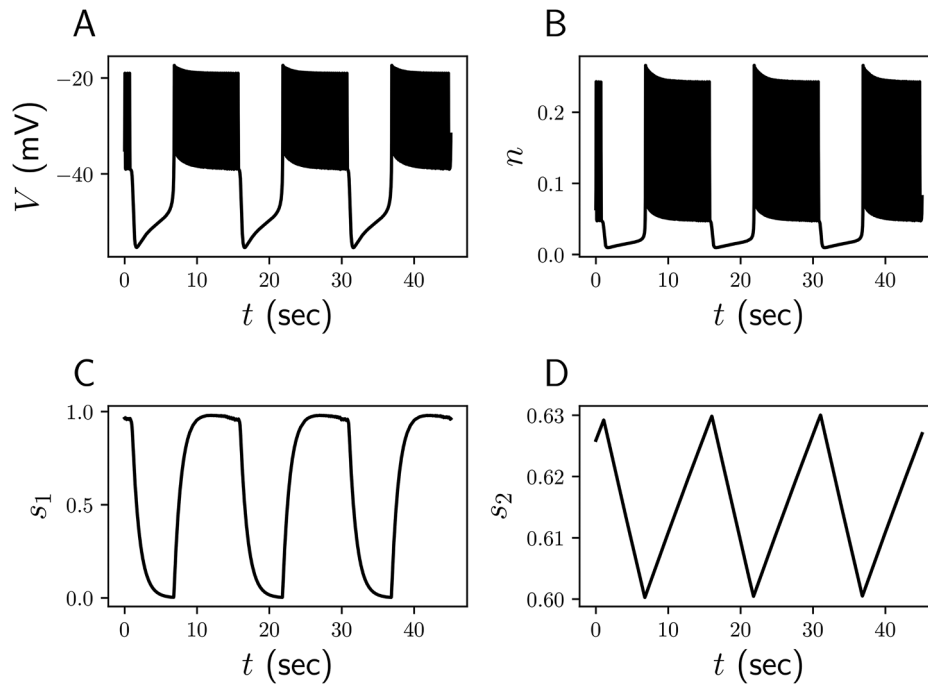


**Fig. 1.** Medium bursting time courses. (A, B) Both  $V$  and  $n$  are fast variables in which individual impulses are evident during the burst active phases. (C, D) Time courses of the slow variables  $s_1$  and  $s_2$  do not exhibit impulses, but instead show the integrated effects of bursts of impulses.

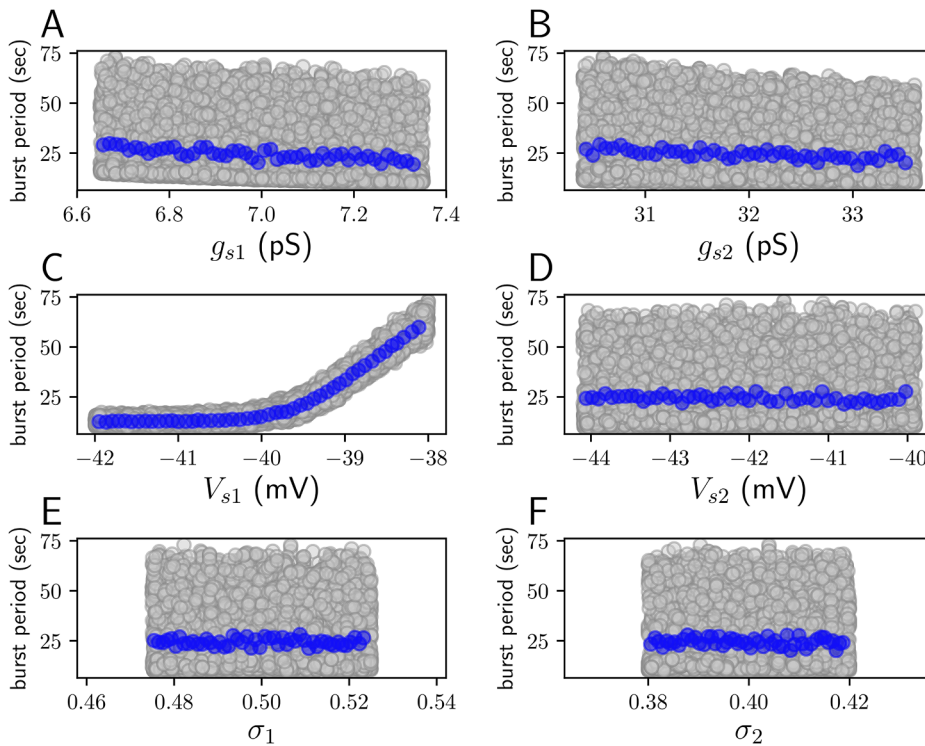


**Fig. 2.** Projections of a 7-dimensional scatter plot along each parameter dimension in the case of medium bursting. Each gray circle is the burst period for the parameter value shown on the abscissa and some combination of values for the remaining 5 parameters. Each blue circle is the mean burst period for the prescribed parameter value (mean of the gray circles in that column).

where,  $f(A)_j$  is the QoI for the parameters corresponding to the  $j$ -th row of the matrix  $A$  and  $f(A_B^{(j)})$  is the QoI for the parameters corresponding to the  $j$ -th row of the matrix  $A_B^{(j)}$ . Our choice of quasi-random sequence is the Sobol' sequence [27], and we use randomized and scrambled Sobol' sequences for a lower discrepancy and better uniformity in sampling the parameter space [21]. To further improve the computational feasibility of the estimation of the total SIs, rather than defining a fixed number of samples for estimation of SI for all of the parameters, we define a convergence criterion such that the estimation of the SI for

a parameter stops in runtime if it converges within an acceptable threshold. Also, we implement the evaluation of the QoI in parallel over multiple CPU cores. The total SIs provide importance of a parameter averaged over the region in the parameter space being analyzed. To see any specific patterns between the QoI and the variation in a significant parameter, we analyze the scatter plots of the QoI versus the parameters using the samples in Sobol' estimation.

The above methods of global sensitivity analysis trade the analytical complexity involved in phase space analysis of a four-dimensional

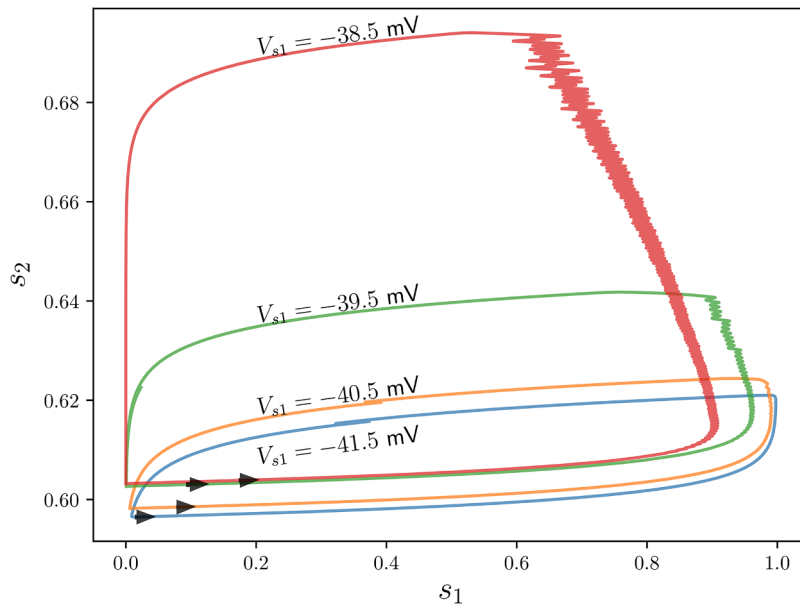


Fig. 3. Projections of the medium bursting orbit onto the plane of the slow variables for four values of  $V_{s1}$  near  $-40$  mV. The range of  $s_2$  values covered begins to increase significantly for  $V_{s1} > -40$  mV.

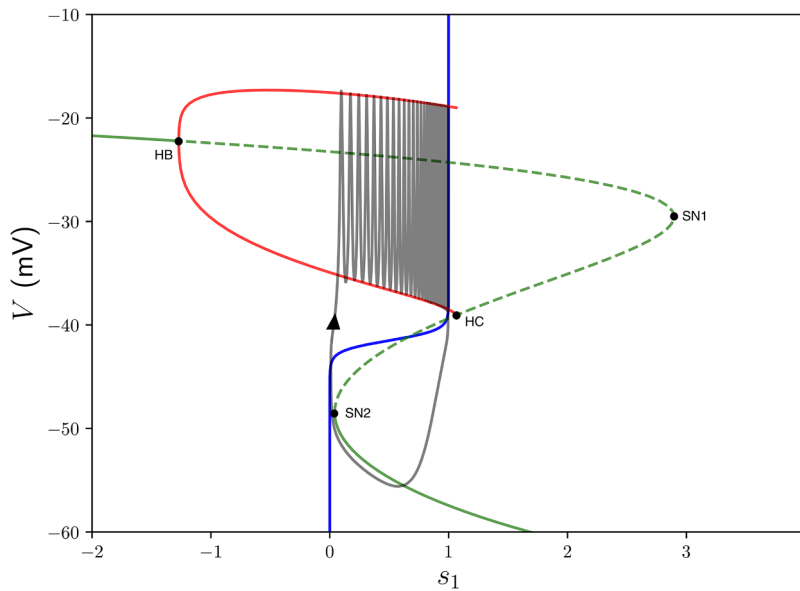
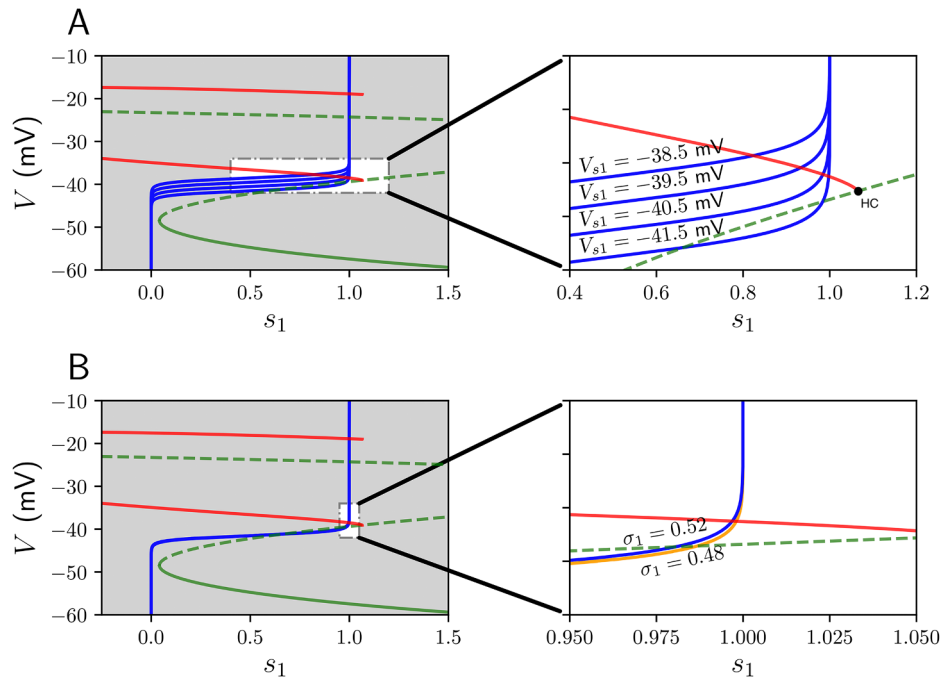


Fig. 4. Fast/slow analysis of bursting with  $V_{s1} = -41.5$  mV and  $s_2 = 0.605$ . Stationary solutions of the  $V - n$  fast subsystem are shown as the green curve (solid = stable, dashed = unstable). Minimum/maximum  $V$  values of periodic solutions are shown as red curves. SN = saddle-node bifurcation, HB = Hopf bifurcation, HC = homoclinic bifurcation.

system, with the complexity of computational feasibility and the precision of the numerical estimation of the QoI, which in our case is the burst period. The burst period is estimated by simulating the system of ODEs (numerically estimated in Python using the LSODA method, which implements the Livermore Solver for ordinary differential equations [23]) over a long time period so that the trajectory converges to oscillations. It is expected that if the burst oscillation is short, then the final time for convergence of the trajectory to oscillations should be low. Therefore, we develop an algorithm which dynamically changes the final time until the trajectory converges to oscillations using a convergence criterion. This improves the computation time for estimating the burst period for thousands of samples of parameters, which is required for the estimation of Sobol' indices.

### 3. Results

The central questions that we address are which of the 6 parameters in the variation set are the most important at setting the burst period, and why are they so important. The variation set consists of those parameters directly related to the  $s_1$  and  $s_2$   $K^+$  currents, which are the ionic currents that package electrical impulses into bursts. The model that we use for bursting in  $\beta$ -cells [1] can produce oscillations that are fast, medium, or slow, depending on the choice of the conductance of the  $s_1$ -current,  $g_{s1}$ . It is likely that different parameters will be important for setting the burst period in these three regimes, so we consider each regime separately, beginning with medium bursting that for many years was the only type of bursting observed in  $\beta$ -cells from intact islets of Langerhans [11,15].



**Fig. 5.** (A) The  $s_1$  nullcline is translated upward when  $V_{s1}$  is increased, moving the intersection with the periodic branch further from the homoclinic bifurcation HC. (B) The effect on the  $s_1$  nullcline of a  $\pm 5\%$  change in  $\sigma_1$  is very small.

**Table 3**

Parameter values for fast bursting, along with their intervals of variation. Also shown is the total of the Sobol’ indices for each parameter.

Parameter	Central value	Interval of variation	$\bar{S}_i$
$g_{s1}$	20 pS	[15, 25]	0.96
$g_{s2}$	32 pS	[24, 40]	0.138
$V_{s1}$	-40 mV	[-43, -39]	0.096
$V_{s2}$	-42 mV	[-43, -39]	0.132
$\sigma_1$	0.5 mV	[0.375, 0.625]	0.069
$\sigma_2$	0.4 mV	[0.3, 0.5]	0.081

**3.1. The medium bursting period is set primarily by the  $s_1$  half-activation value**

We refer to ‘medium bursting’ as bursting with period ranging between 10 s and 75 s. Model parameter values that produce medium bursting with a period of 15 s are given in Table 2, labeled as ‘central values’. The bursting produced with these parameter values is shown in Fig. 1. Electrical impulses are produced during each burst active phase, separated by silent phases when the voltage is low or hyperpolarized. In addition to the membrane potential or membrane voltage ( $V$ ), the figure also shows time courses for the other three variables: the activation variable for delayed-rectifying  $K^+$  channels ( $n$ ), a slow activation variable for another type of  $K^+$  channel ( $s_1$ ), and an even slower activation variable for a third type of  $K^+$  channel ( $s_2$ ). The difference in time scales for the variables is evident from the time courses: impulses appear in  $V$  and  $n$ , but are filtered to produce only slow oscillations in the  $s_1$  and  $s_2$  time courses.

To determine which parameters have the greatest impact on the burst period (defined as the sum of one active and one silent phase), we perform a global sensitivity analysis. A subset of parameters is examined here, focusing on parameters involved in the dynamics of the two slow variables of the model,  $s_1$  and  $s_2$ . Because of the timescale of these variables, changes in their dynamics will have the largest impact on the burst period. The six parameters that we examine are: the maximal conductances of the slowly-activated ionic currents ( $g_{s1}$  and  $g_{s2}$ ), the voltage for half-activation of these currents ( $V_{s1}$  and  $V_{s2}$ ), and

the slopes of the activation curves for the slow currents ( $\sigma_1$  and  $\sigma_2$ ). Here, smaller values of  $\sigma$  yield larger slopes. Each of these six parameters is varied by  $\pm 5\%$  of its central value in the sensitivity analysis, so the sampling is done in a six-dimensional hypercube about the central point in parameter space. At each point a computer simulation of the model is performed, and the period of the resulting medium bursting oscillation is determined. Addition of the period to the six-dimensional parameter space yields a 7-dimensional scatter plot. For visualization purposes, we examine the projections of the high-dimensional scatter plot along each parameter dimension. Thus, we obtain six projected scatter plots, shown in Fig. 2. In each case, the mean burst period is shown in blue. It took approximately 13.5 h of computer time to obtain this data and to subsequently conduct the global sensitivity analysis.

An examination of the scatter plot projections indicates that changes in five of the six parameters have little impact on the mean or the range of variation of burst period. There is one parameter, however, that has a clear effect on the burst period. For this parameter,  $V_{s1}$  (the half-activation level for the  $s_1$  current), the period increases dramatically for  $V_{s1} > -40$  mV. In fact, the dramatic increase in burst period for small changes in  $V_{s1}$  is an indication that some slow process has been engaged and that a fast/slow analysis could be applied to understand the mechanism for the dramatic change in period. That  $V_{s1}$  is the most sensitive parameter is quantified by the total Sobol’ index ( $\bar{S}_i$ ). As shown in Table 2, this sensitivity metric is much larger for  $V_{s1}$  than for any of the other parameters. In fact, it is nearly 100 times larger than the nearest competitor,  $g_{s1}$ , which was a parameter identified in an earlier study to be of importance in setting the period of medium bursting [1].

Why does the  $s_1$  half-activation value have such a large influence on burst period for  $V_{s1} > -40$  mV? To begin to understand this, we project the burst trajectory onto the plane of the slow variables, i.e., the  $s_1s_2$ -plane (Fig. 3). This is done for four values of  $V_{s1}$  near -40 mV. For  $V_{s1} = -41.5$  mV (blue trace) the closed burst orbit extends over the maximum range of  $s_1$ , 0 to 1. In contrast, it extends over a very small range of  $s_2$ , from 0.59–0.62. This difference reflects the much larger time constant for  $s_2$  versus that of  $s_1$ . The orbit for  $V_{s1} = -40.5$  mV is similar. However, for  $V_{s1} = -39.5$  mV and particularly  $V_{s1} = -38.5$  mV, the  $s_2$  range covered is several times greater. Given the large  $s_2$  time

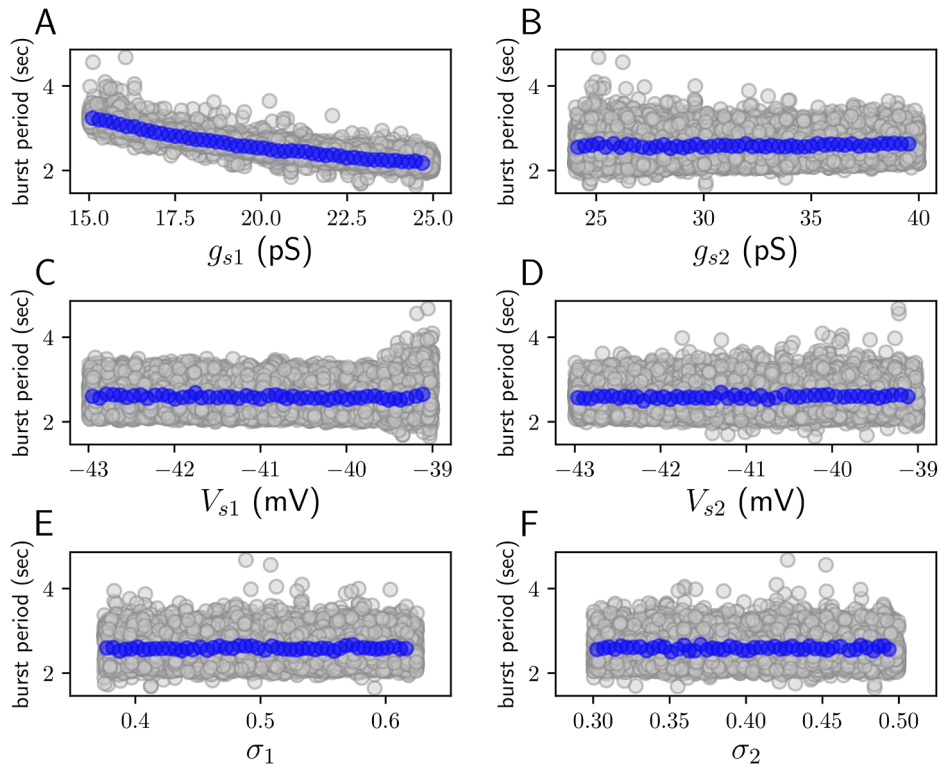


Fig. 6. Scatter plot projections for the case of fast bursting. The blue circles indicate mean values.

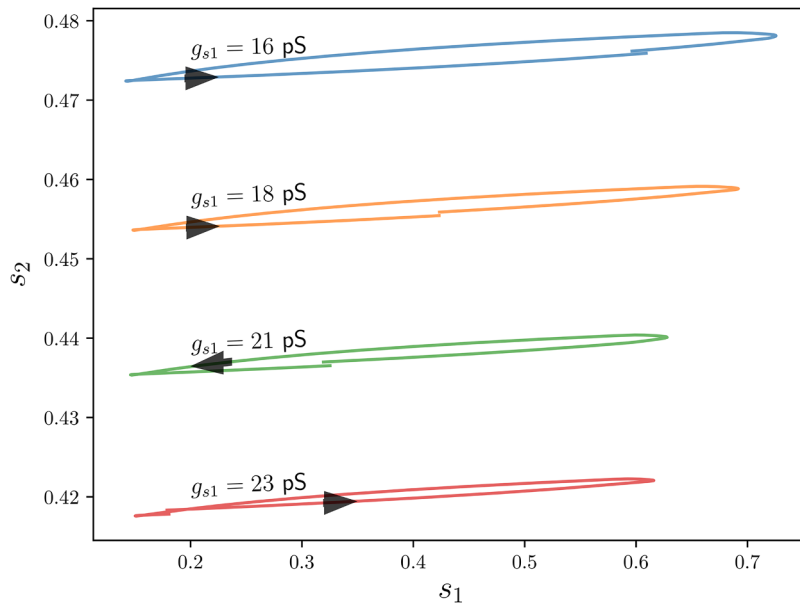


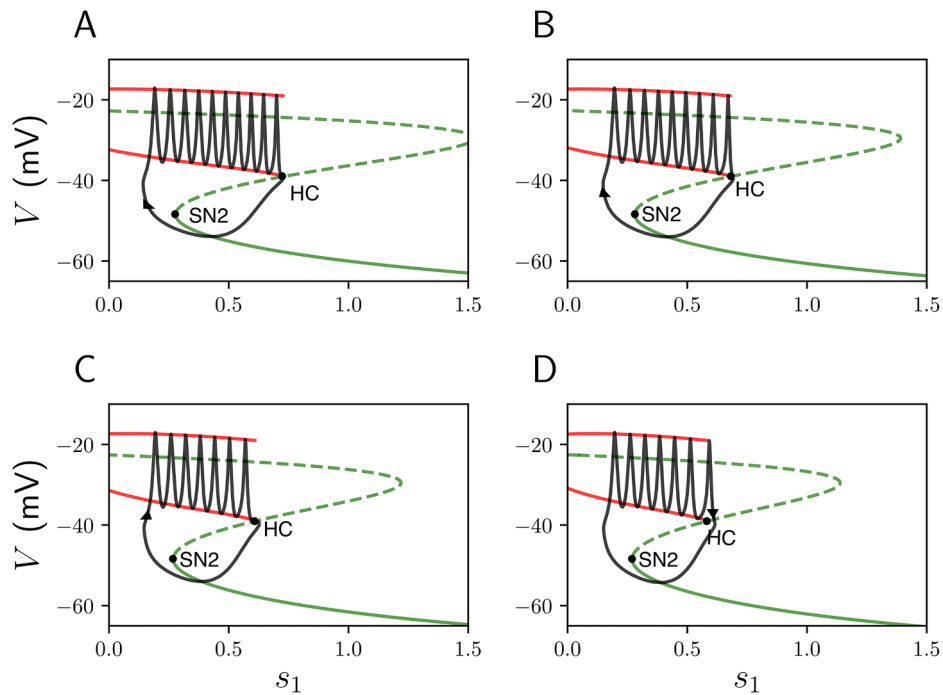
Fig. 7. Four fast bursting orbits projected into the plane of the slow variables. The range of  $s_1$  values covered increases with smaller values of  $g_{s1}$ .

constant, this larger coverage corresponds to a much larger burst period. Thus, the reason for the larger burst period when  $V_{s1} > -40$  mV is the large range of  $s_2$  values taken on during the oscillation. But why does this happen? To answer this question we perform a fast/slow analysis.

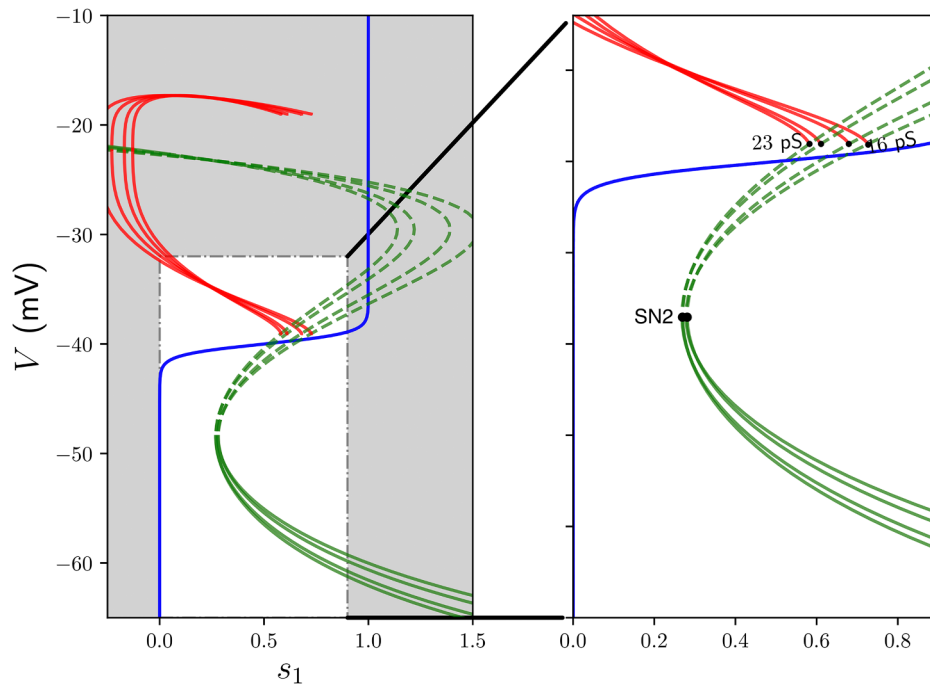
We begin by clamping the slowest variable to the value taken on during the beginning of the burst active phase. For the case  $V_{s1} = -41.5$  mV this is  $s_2 = 0.605$ . We then construct a bifurcation diagram using the other slow variable,  $s_1$ , as the bifurcation parameter. There is a Z-shaped branch of equilibria of the  $V - n$  fast subsystem called the critical manifold, projected into the  $s_1V$ -plane in green in

Fig. 4. Stable branches are indicated with solid curves, while unstable branches are shown as dashed curves. Changes in stability occur at two saddle-node bifurcations (SN1 and SN2) and a Hopf bifurcation (HB). At the HB, a branch of stable periodic solutions emerges (red), reflecting continuous trains of impulses. The periodic branch terminates at a homoclinic bifurcation (HC) where it connects with a branch of saddle points. In Fig. 4, the periodic branch is shown as a curve for the minimum  $V$  and another for the maximum  $V$  taken on during the oscillation.

The next step in the fast/slow analysis is to add back the  $s_1$  dynamics (while keeping  $s_2$  fixed), now thinking of the bifurcation diagram as a



**Fig. 8.** Fast/slow analysis of fast bursting with four different values of  $g_{s_1}$  and  $s_2$  clamped at its average value in each case. (A)  $g_{s_1} = 16$  pS,  $s_2 = 0.475$ , (B)  $g_{s_1} = 18$  pS,  $s_2 = 0.456$ , (C)  $g_{s_1} = 21$  pS,  $s_2 = 0.438$ , (D)  $g_{s_1} = 23$  pS,  $s_2 = 0.420$ . The interval of bistability is smaller for larger values of  $g_{s_1}$ .



**Fig. 9.** Superposition of four critical manifolds for the case of fast bursting, corresponding to  $g_{s_1} = 16$  pS, 18 pS, 21 pS, and 23 pS. As  $g_{s_1}$  increases, the interval of bistability between the bottom stationary branch and the periodic branch (interval from SN2 to HC) decreases. In all cases, the  $s_1$  nullcline (blue) intersects the critical manifold on the middle stationary branch, below the periodic branch. The right panel is a blow up of the left.

generalized  $V$ -nullcline. The  $s_1$ -nullcline (blue) is then superimposed, along with the burst trajectory (black; Fig. 4). During the silent phase when  $V$  is low, the trajectory moves leftward along the bottom branch of the critical manifold. Once this terminates at SN2, the trajectory moves to the spiking branch at the initiation of the burst active phase. Now on the opposite side of the  $s_1$ -nullcline, the trajectory moves rightward. As it approaches the  $s_1$ -nullcline, the rightward motion slows down and the trajectory falls off the spiking branch at its termination at

HC. This is the end of the burst active phase and the beginning of the silent phase. This bursting oscillation, driven by slow variation in  $s_1$ , relies on the interval of bistability of the fast subsystem between SN2 and HC. It also relies on the fact that the  $s_1$ -nullcline does not intersect the bottom branch of the critical manifold, and intersects the spiking branch only near the HC bifurcation (Fig. 5,  $V_{s_1} = -41.5$  mV). When  $V_{s_1}$  is increased, the  $s_1$ -nullcline is translated upwards, so that its intersection with the spiking branch is further from the HC (Fig. 5A). In the

**Table 4**  
Parameter values for slow bursting, along with their intervals of variation. Also shown is the total of the Sobol’ indices for each parameter.

Parameter	Central value	Interval of variation	$\bar{S}_i$
$g_{s1}$	3 pS	[2.85, 3.15]	0.0225
$g_{s2}$	32 pS	[30.4, 33.6]	0.287
$V_{s1}$	-40 mV	[-42, -38]	0.663
$V_{s2}$	-42 mV	[-44.1, -39.9]	0.0036
$\sigma_1$	0.5 mV	[0.475, 0.525]	0.0032
$\sigma_2$	0.4 mV	[0.38, 0.42]	0.0018

two cases of  $V_{s1} = -39.5$  mV and  $-38.5$  mV, the intersection is sufficiently far away so that the trajectory would get stuck here if  $s_2$  remained clamped. That is, there would be no bursting since the trajectory would not escape the active phase. It is the dynamics of  $s_2$  that, in these cases, enables bursting. Once the trajectory stalls near the intersection on the spiking branch, it is the slow increase in  $s_2$  that becomes key. This increase shifts the critical manifold leftward, moving the intersection closer to the HC. Eventually, the distance between the two is so small that the trajectory can escape, ending the active phase. The increase in the value that  $s_2$  must take on is the reason for the larger excursion in the  $s_1s_2$ -plane in Fig. 3 for  $V_{s1} = -39.5$  mV and  $-38.5$  mV. Since  $s_2$  changes on a much slower time scale than  $s_1$ , it is also the reason that the burst period is much greater for values of  $V_{s1} > -40$  mV.

This analysis explains the sensitivity to the parameter  $V_{s1}$  revealed in the global sensitivity analysis, but what about the insensitivity to  $\pm 5\%$  changes in  $g_{s1}$ ,  $g_{s2}$ ,  $V_{s2}$ ,  $\sigma_1$ , and  $\sigma_2$ ? Changing  $g_{s1}$  or  $g_{s2}$  varies the slope of the slow manifold, and thus the location of the HC, but the effect on the burst period is minor for the  $\pm 5\%$  variation in these parameters. Changes in  $\sigma_1$  affect the slope of the  $s_1$ -nullcline, and thus the location of the intersection with the periodic branch of the critical manifold. But this change in location is small, and so too is its effect on the burst period. This is demonstrated in Fig. 5B, where  $s_1$  nullclines are shown for  $\sigma_1$  at  $\pm 5\%$  of its central value. Changes in  $V_{s2}$  and  $\sigma_2$  affect the range of values taken on by  $s_2$ , affecting the slow manifold, and thus the HC. None of these effects are large enough to have a noticeable

impact on the burst period (Fig. 2).

### 3.2. A different parameter has the primary impact on fast bursting period

Fast bursting refers to bursting with a period of 10 s or less. Fast bursting periods of 2–5 s have been observed in single-cell electrophysiological studies [13,18] as well as in intact islets following the application of acetylcholine [6,10]. The central parameter values for fast bursting, with a period of 3 s, are given in Table 3. We restrict the parameter variation so that bursting remains fast, with period  $< 10$  s, and for this reason the interval of variation of  $V_{s1}$  and  $V_{s2}$  is centered about  $-41$  mV rather than their central values. Also, since  $\pm 5\%$  parameter variation did not give a large range of burst periods in fast bursting, we increased the parameter variation to  $\pm 25\%$  in all of the remaining parameters. The intervals of variation are shown in Table 3.

The effects of parameter variation on the burst period are shown in the projected scatter plots of Fig. 6. It took approximately 7 h of computer time to obtain this data and to subsequently conduct the global sensitivity analysis. In this case, only the parameter  $g_{s1}$  has a large effect on the burst period. This is most evident from an examination of the means (blue circles), but also the range of variation of the burst period is much greater when  $g_{s1}$  is included in the set of varied parameters (as it is in all panels except panel A) than when it is clamped (panel A). The greater impact of  $g_{s1}$  on burst period is also demonstrated by the total of the Sobol’ indices,  $\bar{S}_i$ . This is nearly 7 times greater for  $g_{s1}$  than it is for the nearest competitor,  $V_{s1}$  (Table 3). Thus, the most significant parameter for fast bursting is different than that for medium bursting.

To understand the reason for the large influence of  $g_{s1}$  on the burst period we first project the burst trajectory onto the plane of the slow variables for several values of  $g_{s1}$  (Fig. 7). Unlike the case for medium bursting, the range of  $s_1$  values taken on during fast bursting is not maximal. In particular,  $s_1$  never reaches its maximal value of 1. Instead, as  $g_{s1}$  is decreased the trajectory reaches larger and larger values. The need to attain larger  $s_1$  values to generate sufficient ionic current for active phase termination is the reason for the increase in the burst period for small  $g_{s1}$  values in Fig. 6. In contrast, the range of values of  $s_2$

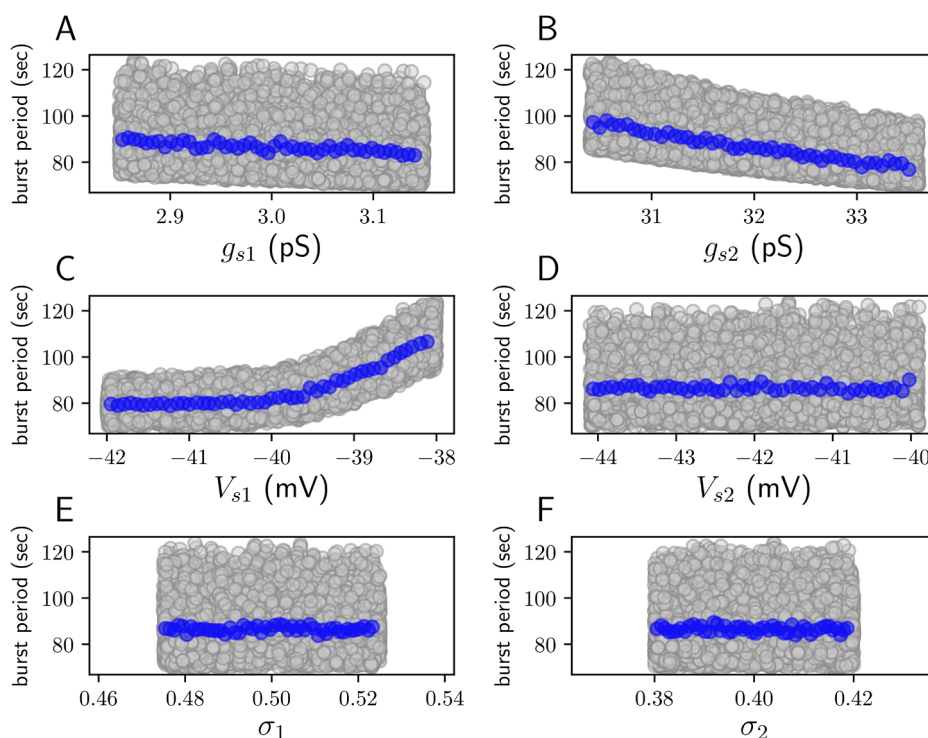


**Fig. 10.** Scatter plot projections for the case of slow bursting. The blue circles indicate the mean values.

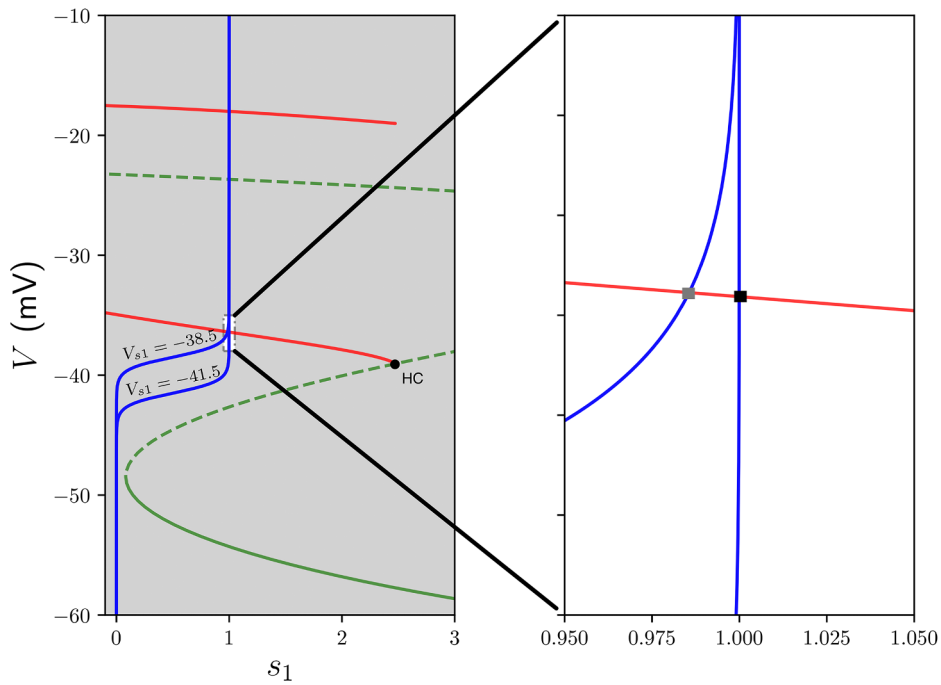


**Fig. 11.** In the fast/slow analysis of slow bursting, the effect of increasing  $V_{s1}$  is to translate the  $s_1$  nullcline upward. For  $V_{s1} > -40$  mV, this results in an intersection of the nullcline with the periodic branch of the fast subsystem. The larger the value of  $V_{s1}$  the deeper the intersection in the periodic branch (shown in the blow up on the right). Nullclines are shown for two values of  $V_{s1}$ , one value less than  $-40$  mV and the other greater than  $-40$  mV. In addition,  $g_{s2} = 30.5$  pS and  $s_2 = 0.636$ .

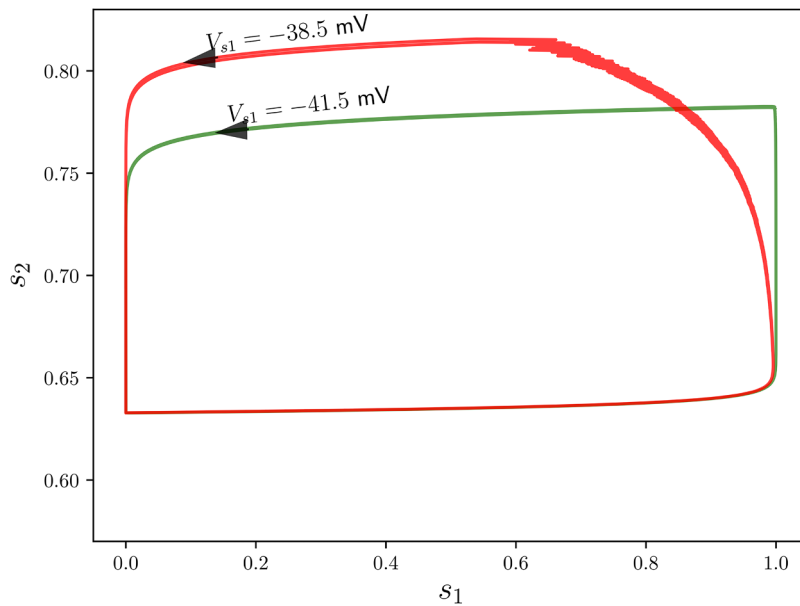


**Fig. 12.** During slow bursting,  $s_2$  must reach a larger value to terminate a burst active phase when  $V_{s1}$  is smaller. The  $s_2$  value reached during the silent phase is the same for both values of  $V_{s1}$ . Therefore, the range of values taken on by  $s_2$  is greater when  $V_{s1}$  is larger and  $V_{s1} > -40$  mV. For this example,  $g_{s2} = 30.5$  pS.

taken on during a burst changes little with  $g_{s1}$ , indicating that this is not a major factor in the change in burst period with  $g_{s1}$ . To understand why the  $s_1$  range changes with  $g_{s1}$  we again turn to fast/slow analysis.

As before, bifurcation diagrams of the fast subsystem are shown in Fig. 8, now with four different values of  $g_{s1}$ . In each case, the second slow variable is clamped at its average value taken on during the bursting oscillation. For small values of  $g_{s1}$  there is a large range of bistability that must be traversed to complete one cycle of bursting (Fig. 8A). As  $g_{s1}$  is increased the knees of the critical manifold come

together, as do the SN2 and HC bifurcations. With the reduced interval of bistability, the trajectory spends less time in silent and active phases, resulting in smaller burst periods. The critical manifolds for all four cases are overlaid in Fig. 9. Unlike in the case of medium bursting, translating the  $s_1$  nullcline up or down by changing the  $V_{s1}$  parameter has little effect on the bursting. This is because the  $s_1$  nullcline and the periodic branch of the critical manifold never intersect when the bursting is fast, so that dynamic changes in  $s_2$  are not needed to get the trajectory out of the active phase.

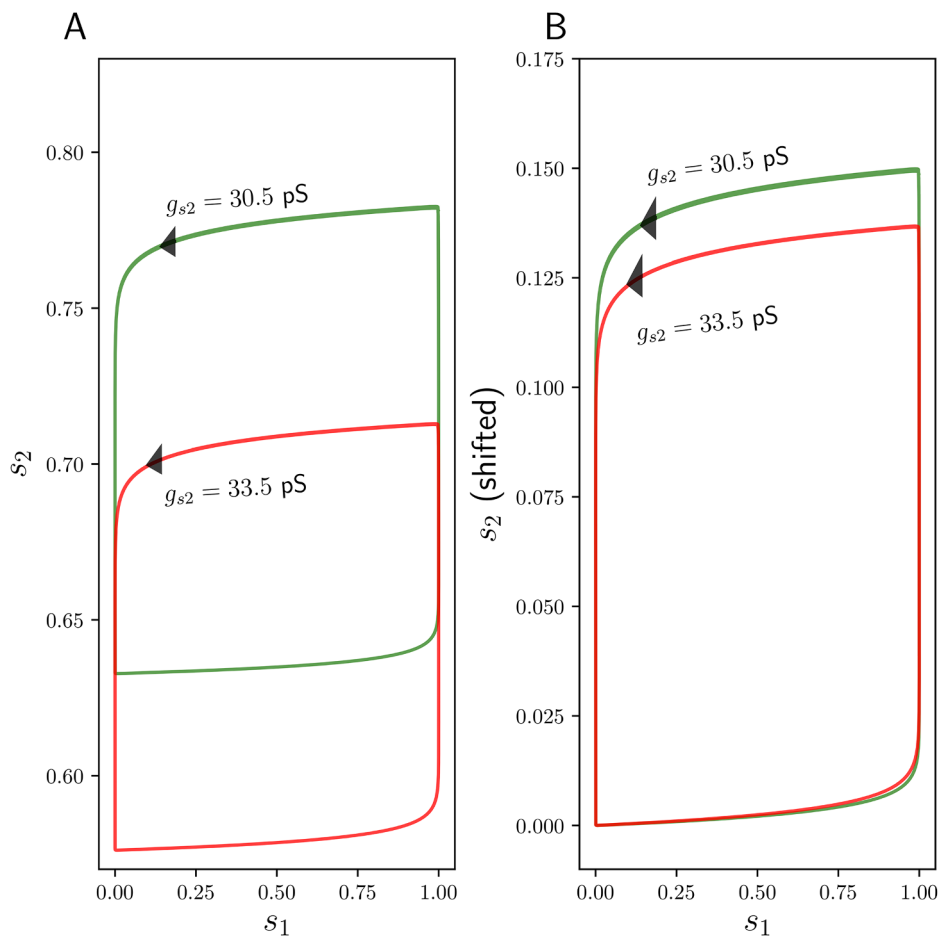


**Fig. 13.** (A) Projections of slow bursting orbits for two values of  $g_{s2}$ . (B) When the orbits are translated so that the minimum  $s_2$  values coincide it is clear that  $s_2$  covers a larger range of values when  $g_{s2}$  is smaller. In this example,  $V_{s1} = -41.5$  mV.

### 3.3. The slow bursting period is sensitive to both $s_1$ and $s_2$ current parameters

We refer to slow bursting as bursting with period greater than 70 s. It is often observed in intact pancreatic islets [20] and occasionally in single  $\beta$ -cells or small clusters of  $\beta$ -cells [1,19,26]. Central model parameter values that produce slow bursting with a period of 1.5 min are given in Table 4, and as before we vary these values  $\pm 5\%$  for sensitivity analysis.

Scatter plot projections from the sensitivity analysis (Fig. 10) show that the parameters having the most impact on burst period are  $g_{s2}$  and  $V_{s1}$ , followed by  $g_{s1}$ . Changes in the other parameter values have little impact. This result is quantified by the total of the Sobol’ indices;  $\bar{S}_i$  is greatest for  $V_{s1}$ , followed by  $g_{s2}$ , and then at a much smaller value for  $g_{s1}$  (Table 4). The indices for other parameters are negligible by comparison. It took approximately 2 hours of computer time to conduct the global sensitivity analysis.

The reason that  $V_{s1}$  has a large impact on burst period when  $V_{s1} > -40$  mV is the same as in the case of medium bursting. Increasing the value of the parameter translates the  $s_1$  nullcline upward, so that the intersection of the nullcline with the periodic branch that occurs for  $V_{s1} > -40$  mV occurs further to the left in the  $s_1$ - $V$ -plane for larger  $V_{s1}$  values (Fig. 11). That is, the intersection is deeper into the periodic branch, so  $s_2$  must increase to a larger value for the burst trajectory to escape the active phase (Fig. 12). During the silent phase,  $s_2$  reaches the same value regardless of the value of  $V_{s1}$  (Fig. 12). Therefore, for  $V_{s1} > -40$  mV,  $s_2$  must cover a larger range of values to produce bursting for larger values of the  $V_{s1}$  parameter, and since the time constant for  $s_2$  is large this extra coverage greatly increases the burst

period.

In the case of medium bursting, and indeed for the first time, the  $g_{s2}$  parameter has a significant impact on the burst period with  $\pm 5\%$  variation from its central value. Why is this the case? When the burst trajectory is projected into the  $s_1$ - $s_2$ -plane for two values of  $g_{s2}$  it is unclear whether changing  $g_{s2}$  changes the range of  $s_2$  values taken on during bursting (Fig. 13A). However, when the orbits are translated so that the minimum  $s_2$  values are equal (Fig. 13B), it becomes clear that  $s_2$  covers a larger range of values for the smaller  $g_{s2}$  value. It is for this reason that the burst period is larger when  $g_{s2}$  is smaller (Fig. 10B).

To understand why  $g_{s2}$  has the effect that it does on the burst period, it is best to analyze the bursting in the  $s_2$ - $V$ -plane, now treating  $s_1$  as a fast variable and  $s_2$  as the slowly-varying parameter. Fig. 14A shows a bifurcation diagram of the  $V, n, s_1$  fast subsystem for two different values of  $g_{s2}$ . For the larger value of the parameter the diagram is shifted leftward, so when the burst trajectory is superimposed (black curves) it is left-shifted in the case of  $g_{s2} = 33.5$  pS. It is not, however, clear why the range of  $s_2$  values covered during the bursting is larger for smaller  $g_{s2}$ . To see this, we focus on the portion of the diagram that covers the bistable region of the fast subsystem. That is, the portion between the left saddle-node bifurcation of the critical manifold and the homoclinic orbit that terminates the periodic branch (Fig. 14B,C). In both panels, the trajectory leaves the bottom branch when the saddle-node is reached, and moves almost vertically to the periodic branch (left vertical portion of the orbits). The active phase terminates and the trajectory moves almost vertically downward from the periodic branch to the lower portion of the critical manifold (right vertical portion of the orbits) when the homoclinic bifurcation is reached. The difference between the  $s_2$  value of the homoclinic bifurcation and the saddle-node

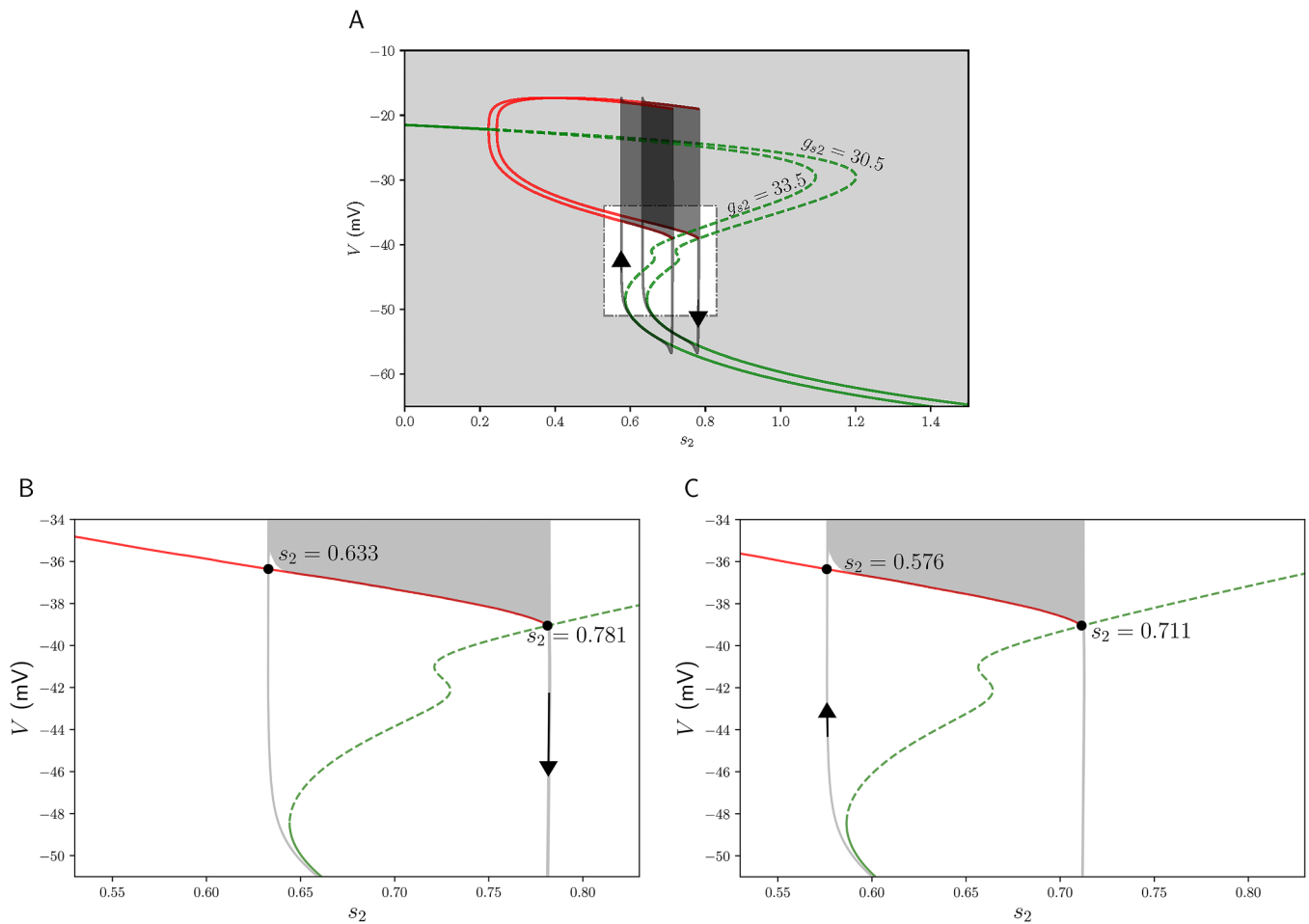


**Fig. 14.** Slow bursting analysis of the  $V, n, s_1$  fast subsystem, with  $s_2$  as the slowly varying bifurcation parameter. (A) Slow manifolds with superimposed burst trajectories for two values of  $g_{s_2}$ . (B) Blow up focusing on the region of bistability, with  $g_{s_2} = 30.5$  pS. The  $s_2$  variable traverses a distance of  $0.781 - 0.633 = 0.148$ . (C) Blow up with  $g_{s_2} = 33.5$  pS. The  $s_2$  variable traverses a distance of  $0.711 - 0.576 = 0.135$ . In both cases,  $V_{s_1} = -41.5$  mV.

bifurcation, which is the interval of bistability in the fast subsystem, thus determines the range of values taken on by  $s_2$  during bursting. This range of values is larger for smaller values of  $g_{s_2}$ .

#### 4. Discussion

Understanding the behavior of a parameterized model is facilitated by knowing which parameters most affect the model’s behavior and why they have these effects. The various forms of global sensitivity analysis were developed to achieve the first task of identifying key parameters [16,25,28], while a host of mathematical tools is available for achieving the second task of identifying the means of action of a parameter. In the case of multi-timescale systems, the tool often used is fast/slow geometric analysis [2,4,24]. We have demonstrated how the two mathematical tools can be interwoven in a synergistic way. Prior fast/slow analysis of our model system indicated that there were three distinct regimes for bursting behavior: a fast regime in which the  $s_1$  variable drives the oscillations, a slow regime where  $s_2$  drives the rhythm, and an intermediate regime where the two slow variables share the role of driving the oscillations [1]. In this prior analysis, changes in the parameter  $g_{s_1}$  were used to move the system from one regime to another, because of its observed impact on the burst period. The effects of changing other parameters were not systematically explored.

In this report, the use of global sensitivity analysis to identify important parameters within each behavioral regime confirmed the importance of the  $g_{s_1}$  parameter, but also revealed other important parameters. It is noteworthy that the most important parameters differed

among the regions of parameter space that produced the different forms of bursting. In the case of fast bursting,  $g_{s_1}$  had the most impact on the burst period, supporting the use of this parameter in [1]. Indeed, none of the remaining five parameters that were analyzed had a systematic effect on the burst period. Use of fast/slow analysis demonstrated that the large effect of  $g_{s_1}$  could be understood in terms of its effect on the critical manifold; larger values of  $g_{s_1}$  resulted in smaller regions of bistability. In the case of medium bursting, global sensitivity analysis revealed that the  $V_{s_1}$  parameter had a much greater effect on the burst period than did the next competitor,  $g_{s_1}$ . However, this was only true for values of  $V_{s_1}$  greater than  $-40$  mV. The basis of this unexpected result was again revealed through a fast/slow analysis; for  $V_{s_1} > -40$  mV an increase in the parameter shifted the intersection of the  $s_1$  nullcline deeper into the periodic branch of the fast subsystem. Without the use of global sensitivity analysis it is quite possible that this phenomenon would have been missed, and without the fast/slow analysis the basis of the phenomenon would certainly have remained a mystery. Finally, in the case of slow bursting, the previously identified parameter  $g_{s_1}$  was not even among the two most important parameters identified through global sensitivity analysis,  $V_{s_1}$  and  $g_{s_2}$ . The fast/slow analysis revealed that  $V_{s_1}$  had an effect over the same range of values as with medium bursting, and for the same reason. The other most important parameter,  $g_{s_2}$ , affected the slow burst period much in the same way as changes in  $g_{s_1}$  affected the fast burst period, by changing the size of the region of bistability. However, for slow bursting the fast subsystem was extended to include the  $s_1$  variable, and the interval of bistability was described in terms of the  $s_2$  variable rather than the  $s_1$  variable. Again, global

sensitivity analysis and fast/slow analysis were synergistic in identifying key parameters and in understanding why they are key.

Rather than searching for key parameters, one could ask what effect changes in a specific parameter has on the behavior of the system. Indeed, this was the question asked in a prior study that combined global sensitivity analysis with fast/slow geometric analysis [14]. As shown in that study, and is clear from the present study, the answer to the question depends on the context. That is, it depends on where the system lies in parameter space. Changes in  $g_{s1}$  have a significant impact on the burst period when the bursting is in the fast or medium regime, but not when bursting is in the slow regime. As discussed in [14], this is important to realize when making model predictions for experimental testing; since it is exceedingly rare to know the values of all or most of the parameters in a biological system, model predictions may fail not because the model is wrong, but because the system is in a region of parameter space that is significantly different from that of the model. Realizing the full range of behaviors of the model prior to experimental testing is therefore beneficial.

### Declaration of competing interest

The authors declare that there is no conflict of interest.

### Acknowledgments

This work was supported by National Science Foundation grant DMS-1612193 to R. Bertram.

### Supplementary material

Supplementary material associated with this article can be found, in the online version, at [10.1016/j.mbs.2019.05.004](https://doi.org/10.1016/j.mbs.2019.05.004)

### References

- [1] R. Bertram, J. Preville, A. Sherman, T.A. Kinard, L.S. Satin, The phantom Burster model for pancreatic  $\beta$ -cells, *Biophys. J.* 79 (2000) 2880–2892.
- [2] R. Bertram, J. Rubin, Multi-timescale systems and fast-slow analysis, *Math. Biosci.* 287 (2017) 105–121.
- [3] R. Bertram, A. Sherman, A calcium-based phantom bursting model for pancreatic islets, *Bull. Math. Biol.* 66 (2004) 1313–1344.
- [4] R. Bertram, A. Sherman, Negative calcium feedback: The road from Chay-Keizer, in: S. Coombes, P.C. Bressloff (Eds.), *Bursting: The Genesis of Rhythm in the Nervous System*, World Scientific, Singapore, 2005, pp. 19–48.
- [5] R. Bertram, A. Sherman, L.S. Satin, Metabolic and electrical oscillations: partners in controlling pulsatile insulin secretion, *Am. J. Physiol.* 293 (2007) E890–E900.
- [6] S. Bordin, A.C. Boschero, E.M. Carneiro, I. Atwater, Ionic mechanisms involved in the regulation of insulin secretion by muscarinic agonists, *J. Membrane Biol.* 148 (1995) 177–184.
- [7] R.J. Butera Jr., J. Rinzel, J.C. Smith, Models of respiratory rhythm generation in the pre-Bötzinger complex. i. bursting pacemaker neurons, *J. Neurophysiol.* 82 (1999) 382–397.
- [8] C.C. Canavier, J.W. Clark, J.H. Byrne, Simulation of the bursting activity of neuron  $r_{15}$  in aplysia: role of ionic currents, calcium balance, and modulatory transmitters, *J. Neurophysiol.* 66 (1991) 2107–2124.
- [9] R. Clewley, C. Soto-Trevino, F. Nadim, Dominant ionic mechanisms explored in spiking and bursting using local low-dimensional reductions of a biophysically realistic model neuron, *J. Comput. Neurosci.* 26 (2009) 75–90.
- [10] D.L. Cook, W.E. Crill, D. Porte Jr., Glucose and acetylcholine have different effects on the plateau pacemaker of pancreatic islet cells, *Diabetes* 30 (1981) 558–561.
- [11] D.L. Cook, W.E. Crill, Voltage dependence of rhythmic plateau potentials of pancreatic islet cells, *Am. J. Physiol.* 240 (1981) E290–E296.
- [12] C.A. Deister, M.A. Teagarden, C.J. Wilson, C.A. Paladini, An intrinsic neuronal oscillator underlies dopaminergic neuron bursting, *J. Neurosci.* 29 (2009) 15888–15897.
- [13] L.C. Falke, K.D. Gillis, D.M. Pressel, S. Mislis, Perforated patch recording allows long-term monitoring of metabolite-induced electrical activity and voltage-dependent  $ca^{2+}$  currents in pancreatic islet  $\beta$  cells, *FEBS Lett.* 251 (1989) 167–172.
- [14] P. Fletcher, R. Bertram, J. Tabak, From global to local: exploring the relationship between parameters and behaviors in models of electrical excitability, *J. Comput. Neurosci.* 40 (2016) 331–345.
- [15] J.C. Henquin, H.P. Meissner, W. Schmeer, Cyclic variations of glucose-induced electrical activity in pancreatic  $\beta$  cells, *Pflügers Arch.* 393 (1982) 322–327.
- [16] B. Iooss, P. Lemaître, A review on global sensitivity analysis methods, in: G. Dellino, C. Meloni (Eds.), *Uncertainty Management in Simulation-Optimization of Complex Systems*, Operations Research/Computer Science Interfaces Series, 59 Springer US, 2015, pp. 101–122.
- [17] M.J.W. Jansen, Analysis of variance designs for model output, *Comput. Phys. Commun.* 117 (1–2) (1999) 35–43.
- [18] T.A. Kinard, G. de Vries, A. Sherman, L.S. Satin, Modulation of the bursting properties of single mouse pancreatic  $\beta$ -cells by artificial conductances, *Biophys. J.* 76 (3) (1999) 1423–1435.
- [19] O. Larsson, H. Kindmark, R. Bränström, B. Fredholm, P.-O. Berggren, Oscillations in  $k_{ATP}$  channel activity promote oscillations in cytoplasmic free  $ca^{2+}$  concentration in the pancreatic  $\beta$ -cell, *Proc. Natl. Acad. Sci. USA* 93 (1996) 5161–5165.
- [20] C.S. Nunemaker, M. Zhang, D.H. Wasserman, O.P. McGuinness, A.C. Powers, R. Bertram, A. Sherman, L.S. Satin, Individual mice can be distinguished by the period of their islet calcium oscillations: is there an intrinsic islet period that is imprinted in vivo? *Diabetes* 54 (2005) 3517–3522.
- [21] A.B. Owen, Quasi-monte carlo sampling, *Monte Carlo Ray Tracing: Siggraph 1* (2003) 69–88.
- [22] A.B. Owen, Better estimation of small Sobol sensitivity indices, *ACM T. Model. Comput. S.* 23 (2) (2013) 11.
- [23] K. Radhakrishnan, A.C. Hindmarsh, Description and use of LSODE, the livermore solver for ordinary differential equations, *Lawrence Livermore Natl. Labor. Rep.* (1993).
- [24] J. Rinzel, G.B. Ermentrout, Analysis of neural excitability and oscillations, in: C. Koch, I. Segev (Eds.), *Methods in Neuronal Modeling: From Synapses to Networks*, MIT Press, Cambridge, 1989, pp. 135–169.
- [25] A. Saltelli, P. Annoni, I. Azzini, F. Campolongo, M. Ratto, S. Tarantola, Variance based sensitivity analysis of model output. design and estimator for the total sensitivity index, *Comput. Phys. Commun.* 181 (2) (2010) 259–270.
- [26] P.A. Smith, F.M. Ashcroft, P. Rorsman, Simultaneous recordings of glucose dependent electrical activity and ATP-regulated  $k^{+}$ -currents in isolated mouse pancreatic  $\beta$ -cells, *FEBS Lett.* 261 (1990) 187–190.
- [27] I.M. Sobol', On the distribution of points in a cube and the approximate evaluation of integrals, *Zhurnal Vychislitel'noi Matematiki i Matematicheskoi Fiziki* 7 (4) (1967) 784–802.
- [28] I.M. Sobol', Global sensitivity indices for nonlinear mathematical models and their monte carlo estimates, *Math. Comput. Simul.* 55 (2001) 271–280.